Effect of hot rolling conditions on ridging in 16wt% Cr ferritic stainless steel sheet

by K.A. Annan*, C.W. Siyasiya*, and W.E. Stumpf*

Synopsis

The last seven hot rolling passes of the ferritic stainless steel AISI 430 were simulated on a Gleeble-1500D® thermo-mechanical simulator to investigate the effect of temperature, strain rate, and interpass time on the texture. The compression tests were carried out over a wide range of strain rates ($0.1 s^{-1}$ to $5 s^{-1}$) and temperatures ($1100°C$ to $820°C$) with different interpass times (2, 10, 20, and 30 seconds). The dynamic recrystallization to dynamic recovery transition temperature was determined from examining the relationship between the mean flow stress and the inverse of the deformation temperature in multi-pass tests. It was found that the texture in the central layer of the compressed sample is a strong recrystallization-type. The through-thickness textural and microstructural banding, to a large extent, were found to be weakened by hot deformation in the two-phase ($\alpha + \gamma$) region, as opposed to the single-phase (α) region.

Keywords
ferritic stainless steel, electron backscattering diffraction (EBSD), hot rolling, dynamic recovery, dynamic recrystallization.

Introduction

Countries all over the world are constantly tightening motor vehicle regulations requiring cars to reduce sound (noise) below set limits[1]. Mufflers of car exhausts made of AISI 430 stainless steel are used to moderate the level of noise produced by engines. Fortunately, mufflers are relatively inexpensive to replace, but this could change if the cost of production of the primary material (AISI 430) was to increase. During production the steel is subjected to continuous deformation of the sheet in the rolling direction (RD), which results in a series of ridges aligned in the RD. This phenomenon reduces the aesthetic quality of the steel sheet. Ridging in ferritic stainless steel (FSS) is a result of crystallographic texture in sheets arising from the thermo-mechanical processing during its production[2-5]. During processing, a highly alloyed FSS such as AISI 430 undergoes limited or no phase transformations[6]. During hot rolling, the columnar grains in the as-cast slab become highly elongated bands with a sharp texture[6,7]. It has been established that the deformation in the normal (RD–ND) and rolling (TD-ND) directions (Figure 1) is non-uniform[6]. Certain crystallographic directions are preferred and deformation in those directions is more pronounced

It has also been shown that alignment of similarly oriented grains occurs along the RD in the RD-TD plane and the stronger the alignment, the more severe the ridging. For this reason, it is appropriate to study ridging by analysing the texture derived from electron backscattering diffraction (EBSD) data measured in the RD-TD (or rolling) plane[7-9]. Ridging (sometimes called roping) can be significantly reduced or completely prevented by eliminating microstructural and textural banding, which is the origin of anisotropic flow in mixed-texture metals[7,9]. This can be achieved by modification of the alloy chemistry, casting practice, and the design of the thermomechanical processing schedule. While the first method suggests elimination of the austenite phase during hot rolling, the second method proposes the enhancement of the equiaxed grain ratio during processing[7-9]. The third option, however, makes use of faster recrystallization processes (i.e. both dynamic and static) to reduce the degree of banding. This dynamic recrystallization (DRX) process in 16 wt% Cr ferritic stainless steel is affected by the accompanying partial transformation during hot rolling and, therefore, is influenced by the hot rolling conditions during this processing stage. For BCC metals such as AISI 430, cross slip and climb of dislocations occurs
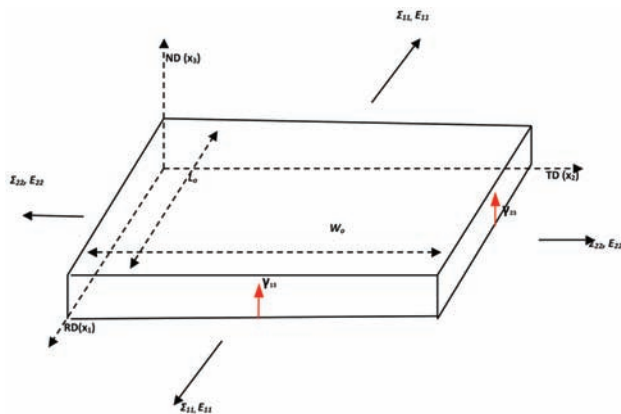
Figure1—Schematic representation of a small region of a sheet and the coordinate system used[6]

with relative ease, which leads to a decrease in dislocation density when dislocations encounter each other and diminish at new slip. This results in low dislocation density during hot working and eventually only dynamic recovery (DRV) occurs[10]. It is, however reported that the decrease in flow stress during hot rolling indicates the occurrence of dynamic recrystallization[10]. This study addresses the contribution of hot rolling parameters to the formation of texture in AISI 430.

Experimental procedure

Experimental material and test procedure

The composition of the AISI 430 used[11] was 0.05 wt% C, 0.39 wt% Si, 16.2 wt% Cr, 0.60 wt% Mn, 0.23 wt% Ni, 0.12 wt% V, 0.030 wt% Co, 0.025 wt% Mo, and 0.019 wt% P. Machined cylindrical specimens for the compression tests were 10 mm in diameter and 15 mm in length. A practical limit of initial diameter (D_o) to initial height (h_o) (i.e. D_o/h_o) of 0.66 was chosen to minimize the barrelling and ensure that no buckling occurred[12]. To decrease the friction and allow uniform deformation, thin tantalum sheets were placed between the compression specimen and the sintered tungsten carbide anvils. Multi-pass hot compression tests were performed on the Gleeble-1500D® thermo-mechanical simulator with pass strains ranging from 0.1112 to 0.1490 together with strain rates from 0.1 s-1 to 5 s-1 and interpass times of 2, 10, 20, and 30 seconds. These strain rates are, however, lower than the industrial strain rates on the Steckel mill. The specimens were initially heated to 1150°C at a rate of 10°C s-1 and homogenized for 5 minutes to eliminate thermal gradients, then cooled at 10°C s-1 to the selected deformation temperature where compression was applied. The multi-pass testing schedule used is illustrated schemat-ically in Figure 2.

Seven compression passes were applied in each test and the temperature was decreased by 30°C between passes. Oxidation of the specimens during testing was prevented by passing a continuous flow of high-purity argon through the system. The as-deformed specimens were immediately helium-quenched to 100°C and then air-cooled to room temperature. The maximum height reduction of all the

specimens was 40 per cent. This ensured that the maximum barrelling factor was kept below 0.9 in all the tests. A friction coefficient of 0.2 was used as a correction factor[12] in calculating the Von Mises flow stress.

Determination of the dynamic recrystallization (DRX) to dynamic recovery (DRV) transition temperature (DR$_{TT}$)

The force-stroke curves obtained from the compression tests were converted into true stress-true strain curves by standard equations[11], as shown in Figure 3.

The mean flow stress (MFS) per pass was calculated from the flow curves (Figure 3) obtained by using the equation:

$$MFS = \frac{1}{\varepsilon_b - \varepsilon_a} \int_{\varepsilon a}^{\varepsilon_b} \sigma \, d\varepsilon \qquad [1]$$
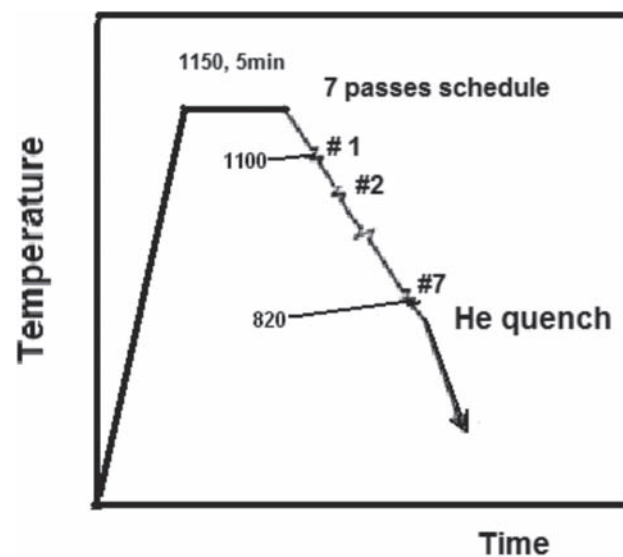

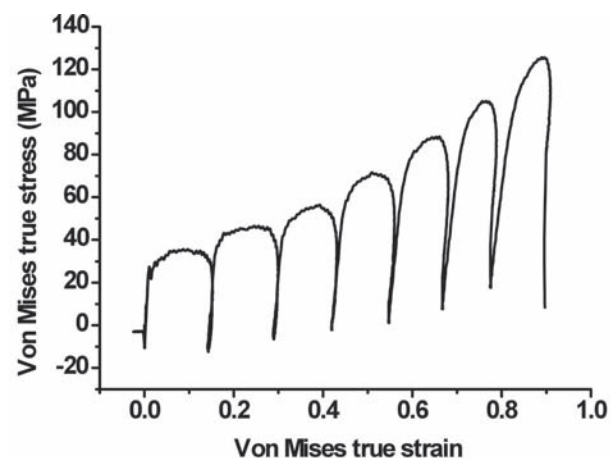Figure 2—Schematic representation of the multi-pass schedule used in the hot compression tests

Figure 3—True stress–strain curves for an AISI 430 stainless steel deformed at a strain rate of 5 s-1 using a 7-pass schedule, starting at 1100°C and ending at 920°C. The inter-pass time was kept constant at 20 seconds

Effect of hot rolling conditions on ridging in16wt% Cr ferritic stainless steel sheet

where ε_a is the initial strain, ε_b is the final strain, and σ is the stress. A typical dependence of mean flow stress on the inverse of absolute temperature obtained from these tests is shown in Figure 4.

The change in linear slope in Figure 4 defines two regions, namely the dynamic recrystallization or DRX region (I) and dynamic recovery region or DRV (II). In region I (high-temperature deformation), dynamic recrystallization takes place as there is no accumulation of strain from pass to pass, and therefore the increase in mean flow stress is due solely to the decrease in temperature. In region II (low-temperature deformation), dynamic recovery takes place. Strain is accumulated from pass to pass within this region and hence the increase in the mean flow stress occurs more rapidly with decreasing temperature.

Sample preparation

The deformed specimens were cut symmetrically into two parts parallel to the compression axis. Central regions of the specimens that experienced the largest localized deformation were chosen as the investigation area. A systematic range of orientation distribution functions (ODFs) from electron backscattered diffraction (EBSD) determinations across the sectioned specimens showed the clearest recrystallization texture in these central areas. The samples were mounted in a plastic resin, adequately ground, and mechanically polished to a 3 μm diamond finish. This was done to ensure that the surface finish was suitable for diffraction[13]. The samples were then removed from the resin and electro-polished at 0.2 A and 20 kV for 20 seconds in 95 per cent ethanol and 5 per cent perchloric acid to remove the mechanically disturbed layer.

Texture measurement and analysis

EBSD measurements, with a step size of 10 per cent of the grain size, were performed on a region of the deformed sample equivalent to the rolling plane of the sheet (RD x TD). The (RD x TD) area was carefully chosen with respect to the

grain size so that at least 1000 or more grains were scanned to have a statistical representation of the orientation of the grains. The samples were tilted at an angle of 70° to the horizontal, which allows more electrons to be diffracted towards the detector[13]. EBSD patterns from a field emission in-lens SEM (FEI Nova Nano® SEM 200) equipped with an EDAX Digiview EBSD Camera were used to determine the crystallographic textures from the mid-thickness regions of the hot compressed samples. A minimum number of seven Kikuchi bands were used to index a pattern during the data collection in order to ensure good reliability of information[13]. An average confidence index of the patterns of more than 0.1 was used, which led to more than 95 per cent of each pattern being indexed correctly. To obtain accurate measurements, misorientations of less than 1.5° were excluded from the data. From these results, orientation distribution functions (ODFs) were obtained using EDAX OIM Software Suite® for data capture and analysis and ϕ_2= 45° sections (Bunge notation). The ODFs were calculated with a 15° Gaussian spread around the ideal orientations.

Results and discussion

Effect of strain rate on the DRX to DRV transition temperature

The mean flow stress increased with increasing strain rate. This was due to a greater restoration by dynamic recovery at the lower strain rates. For example at a strain rate of 0.1 s^{-1}, the deformation time for a strain of 0.1431 was 1.431 seconds. By contrast, at a strain rate of 5 s^{-1}, the deformation time was only 0.0286 seconds for the same strain. Such less-restored and more highly work-hardened austenite supplies more driving force for the dynamic recrystallization and therefore decreases the DR_{TT}[14]. The results presented in Figure 5 demonstrate the effect of strain rate on the DR_{TT} for the steel deformed in the same temperature range (1100°C–920°C), the same interpass times (20 seconds), but at different strain rates (0.1 s^{-1}, 0.5 s^{-1}, 1 s^{-1}, and 5 s^{-1}).
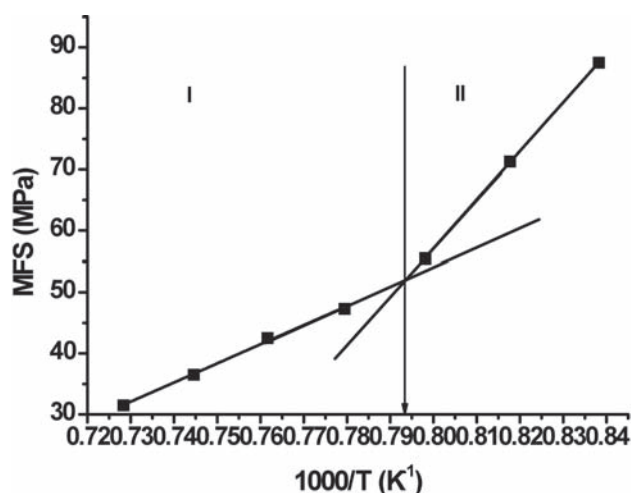

Figure 4—Dependence of the mean flow stress (MFS) on inverse pass temperature during the multi-pass compression testing. AISI 430 stainless steel deformed at strain rate of 0.1 s^{-1}, interpass time of 20 s, and testing temperature from 1100°C–920°C
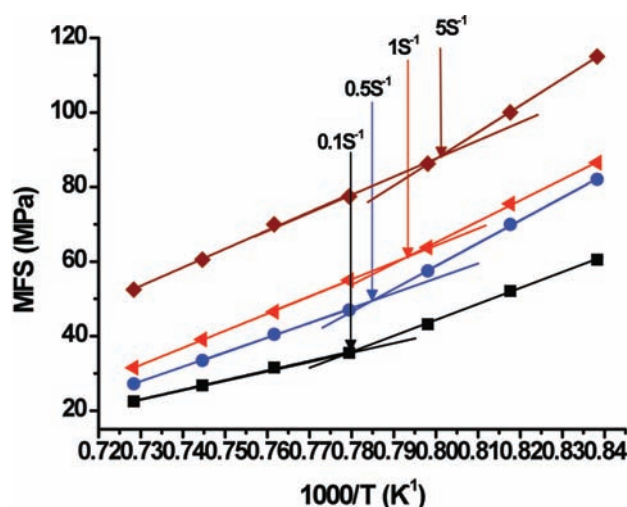

Figure 5—The mean flow stress (MFS) as a function of inverse absolute temperature for 4 samples all deformed at an interpass time of 20 s, temperature range 1100°C to 920°C, and respective strain rates of 0.1 s^{-1}, 0.5 s^{-1}, 1 s^{-1}, and 5 s^{-1}

Figure 6 illustrates the inverse relationship between the strain rate and the DR_{TT} during the compression testing of the samples.

Effect of interpass time on DRX to DRV transition temperature

The DR_{TT} increased with increasing interpass time. At temperatures above the DR_{TT}, the interpass times did not affect the mean flow stress as dynamic recrystallization occurred during deformation and hence no further softening occurred in the interpass time. At deformation temperatures below the DR_{TT}, further softening occurred in the interpass time, due largely to dynamic recovery. Hence, the increase in mean flow stress could be ascribed to the decrease in temperature and the retardation of recrystallization. The dependence of DR_{TT} on interpass time is illustrated in Figure 7 for steels deformed over the same temperature range (1100°C–920°C), same strain rate (0.1 s^{-1}), but different interpass times (2 seconds, 10 seconds, 20 seconds, and 30 seconds). Figure 8 illustrates the relationship between the DR_{TT} and the interpass time.
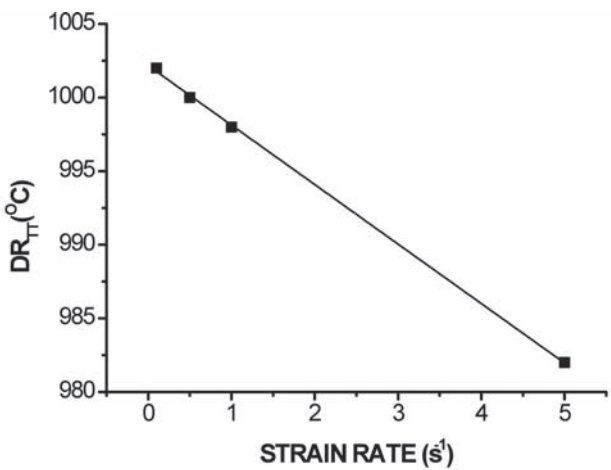

Figure 6—Relationship between the DR_{TT} and the strain rate for the deformation data of Figure 5
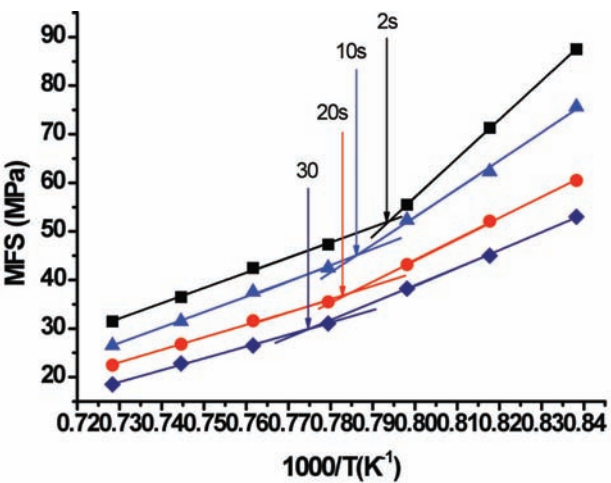

Figure 7—Mean flow stress (MFS) as a function of inverse absolute temperature for samples deformed at different interpass times of 2 s, 10 s, 20 s, and 30 s, same temperature range of 1100°C–920°C set at a constant strain rate of 0.1 s^{-1}

Texture in AISI 430

The hot rolling conditions used for the compression test are as summarized in Table I.

Figure 9 shows important fibres and orientations on the $\phi_2 = 45°$ sections in ODF (Bunge notation), which was used to analyse the EBSD data.
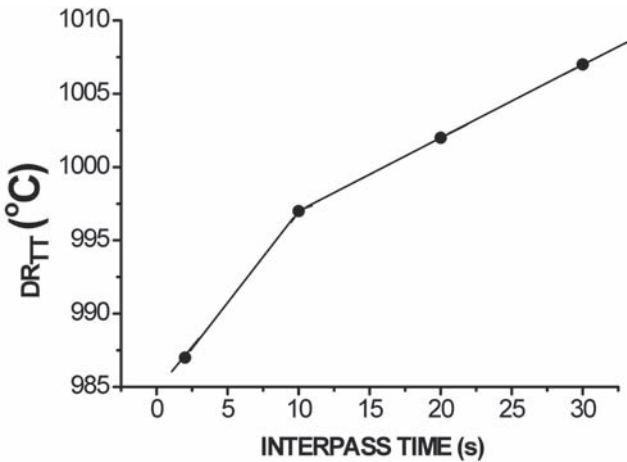

Figure 8—Relationship between the DR_{TT} and the interpass time for the deformation data of Figure 7

Table I

The hot rolling conditions used for the compression tests

Hot rolling Condition	Hot rolling parameters		
	Temperature (°C)	Strain rate (s^{-1})	Interpass time (s)
A	1100–920	5	20
B	1100–920	0.1	2
C	1100–920	0.1	20
D	1000–820	0.1	2

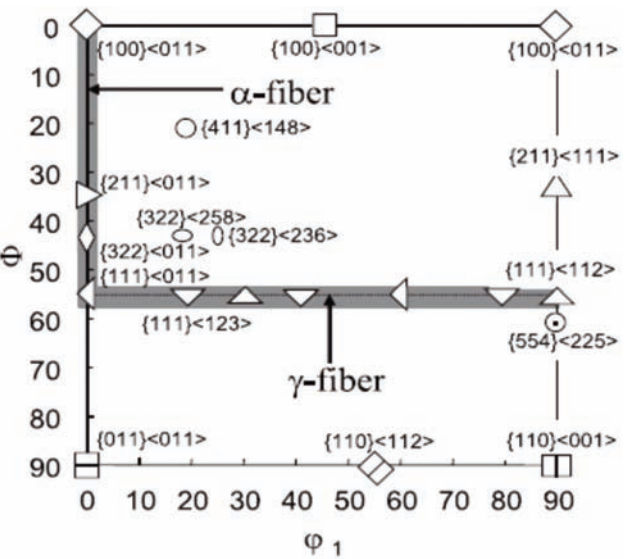Figure 9 – Some important textures and orientations in Euler space (ϕ_2= 45° sections) in Bunge notation used in the texture analysis[14]

Effect of hot rolling conditions on ridging in16wt% Cr ferritic stainless steel sheet

The texture of the hot-rolled steel sheet has a significant influence on the evolution of texture in the cold-rolled as well as the annealed steel sheets[13]. The texture is responsible for the Lankford ratio (r-value). The low r-value of hot-rolled AISI 430 accounts for the poor drawability, which is well-recognized in hot-rolled steel[13-14]. As shown in Figure 10, the texture in the as-received samples is a combination of a strong Goss texture {011}<011>and weak {211}<011> and {211}<111> textures. If these textures are retained in the subsequent cold working and annealing processes, poor drawability of this steel and subsequently ridging and roping could occur[15].

The mean r-value of hot-rolled AISI 430 ferritic stainless steel obtained from the producer was determined by tensile testing to be 0.48, whereas the r-value of the final annealed sample was 1.25. The $\phi_2 = 45°$ sections of the AISI 430 steel deformed at different hot-rolling conditions (Table I) are shown in Figure 11 a-d. The texture of the steel hot-rolled using condition A consists of a strong rotated cube component {100}<001> and a weak α-fibre {111}<110> as shown in Figure 11 (a). This condition represents a combination of a high finishing rolling temperature, high strain rate, and a longer interpass time. The second rolling condition B led to the sharpening of the strong rotated cube component {100}<001> with weaker γ-fibres {111}<123> and {554}<225>, as shown in Figure 11 (b). Increasing the interpass time from 2 seconds (condition B) to 20 seconds (condition C) led to a slight improvement in the γ-fibre.

Condition D has the same rolling parameters as condition B except that the finishing temperature is lower at 820°C instead of 920°C. Condition D resulted in a strong α- fibre textures RD//<110> along with a strong rotated cube {100}<001>. A summary of the analysis of these textures is presented in Table II.
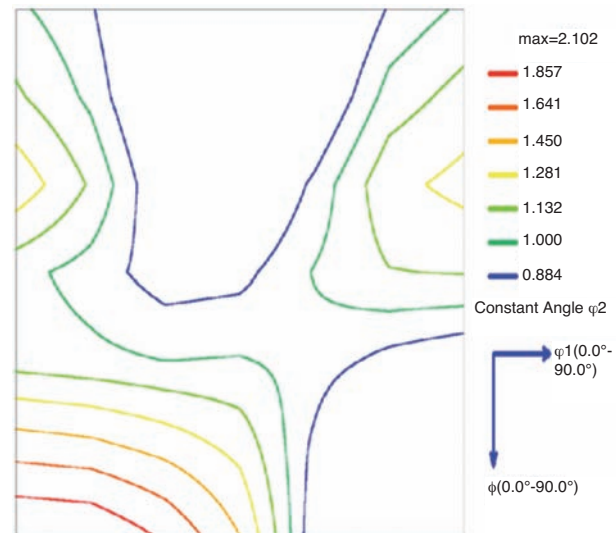

Figure 10—EBSD ODF $\phi_2 = 45°$ RD-TD sections of the industrially hot rolled hot band of AISI 430

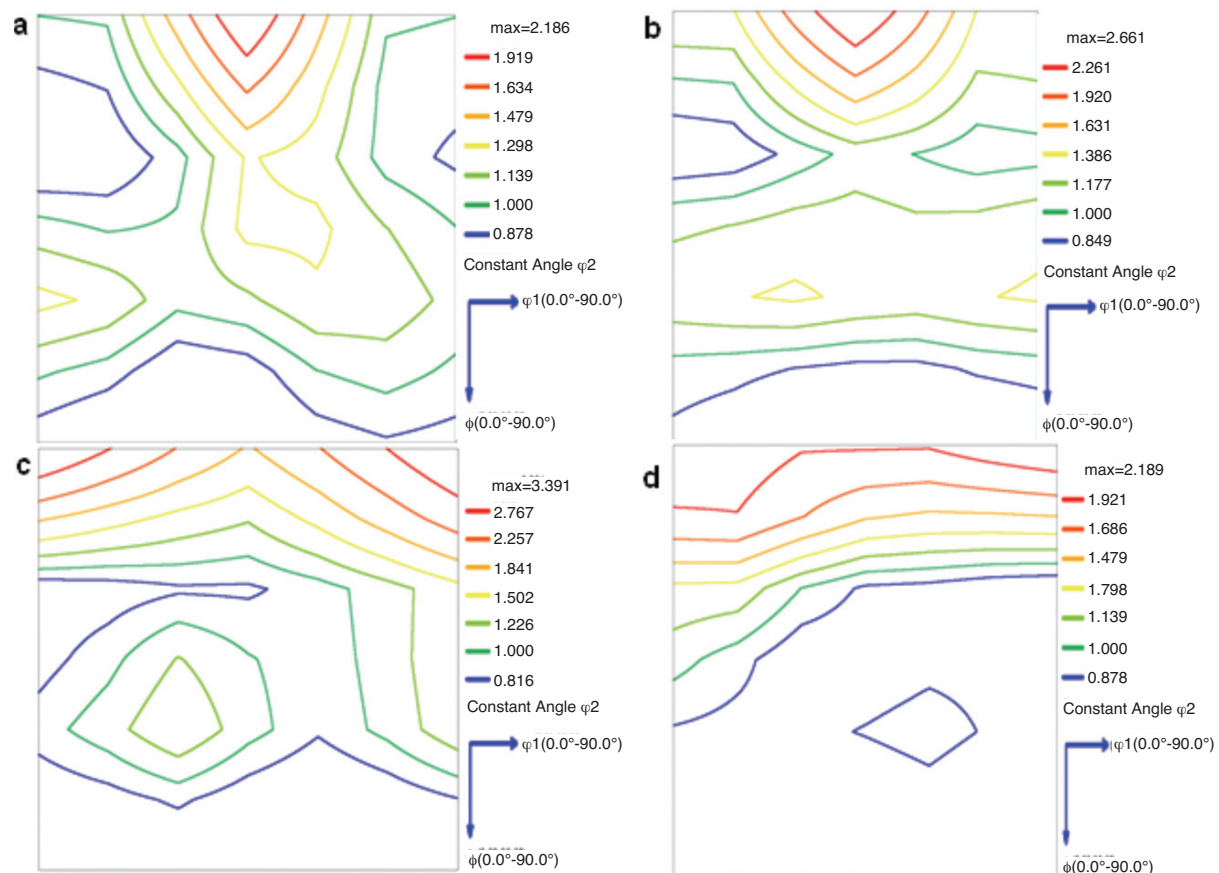**Figure 11—EBSD ODF $\phi_2 = 45°$ RD-TD sections of the AISI 430 samples deformed at (a) condition A (b) condition B (c) condition C (d) condition D, as described in Table I**

Effect of hot rolling conditions on ridging in16wt% Cr ferritic stainless steel sheet

Table II		
Summary of the textures obtained from different hot-rolling conditions		
Conditions	**Description**	**Observed textures**
A	High finishing temp., high strain rate, long interpass time	{100}<001>, {111}<011>,
B	High finishing temp., short interpass time, low strain rate	{100}<001>, {111}<123>, {554}<225>
C	High finishing temp., low strain rate, long interpass time	{100}<011>,{100}<001>, {211}<111> {111}<123>, {554}<225>, {211}<011>
D	Low finishing temp., low strain rate, short interpass time	{100}<011>, {100}<001> {211}<011>, {211}<111>

The dominant textures found in all four different anisothermal simulated hot compression tests were strong α-fibre and rotated cube textures RD//<110> and {100}<001> respectively. However, the as-received hot-rolled steel exhibited only a strong {011}<011> texture without a rotated cube texture.

Conclusions

The following conclusion can be drawn at this stage:

➤ The dynamic recrystallization to dynamic recovery transition temperature was found to decrease with increasing strain rate
➤ The dynamic recrystallization to dynamic recovery transition temperature increased with increasing interpass time
➤ The simulated hot compressed samples exhibited a different texture from the as-received industrial hot rolled steel as a result of the differences in strain rates
➤ Higher finishing rolling temperatures, lower strain rates, and longer interpass times appear to improve the formation of the γ-fibre texture, which contributes to ductility or drawability in this steel. A relatively stronger γ- fibre texture appears to be obtained under this condition.

Acknowledgements

References

1. TRANSPORT AND ENVIRONMENT. New EU vehicle noise limits. December 2011. http://www.transportenvironment.org/sites/te/files/media/2011 12 Noise briefing.pdf

2. CHAO, H.C. Mechanism of anisotropic lamellar fractures. *Transactions of the American Society for Metals*, vol. 2, 1976. pp. 37–50.

3. TAKECHI, H., KATO, H., SUNAMI, T., and NAKAYAMA, T. Mechanism of ridging formation in 17% chromium stainless steel sheet. *Transactions of the Japan Institute of Metals*, vol. 8, 1967. pp. 233–239.

4. SHIN, H.J., AN, J.K., PARK, S.H., and LEE, D.N. The effect of texture on ridging of ferritic stainless steel. *Acta Materialia*, vol. 51, 2003. pp. 4693–4706.

5. ENGLER, O., HUH, M., and TOMÉ, C.N. Crystal-plasticity analysis of ridging in ferritic stainless steel sheets. *Metallurgical and Materials Transactions A*, vol. 36A, 2005. pp. 3127–3139.

6. WU, P.D., JIN, H., SHI, Y, and LLOYD, D.J. Analysis of ridging in ferritic stainless steel sheet. *Materials Science and Engineering,* vol. 423, 2006. pp. 300–305.

7. BROCHU, M., YOKOTA, T., and SATOH, S. Analysis of grain colonies in type 430 ferritic stainless steels by electron back scattering diffraction (EBSD). *ISIJ International*, vol. 37, 1997. pp. 872–877.

8. HARASE, J., OHTA, K., TAKESHITA, T.R., and SCHIMIZU, R. Grain orientation distribution in a hot rolled 17% Cr ferritic stainless steel. *Materials Forum*, vol. 14, 1990. pp. 296–303.

9. BETHKE, K., HOLSCHER, M., and LUCKE, K. Local orientation investigation on the ridging phenomenon in Fe 17% Cr steel. *Materials Science Forum*, vol. 157–162, 1994. pp. 1137–1144.

10. GUR, C.H. and PAN, J. (eds.). Handbook of Thermal Process Modelling of Steels. CRC Press, Boton Raca, Florida, 2009. pp. 93-99.

11. Columbus Stainless. Columbus Technical Data CS430. http://www.columbusstainless.co.za

12. DIETER, G. 1988 Mechanical Metallurgy. SI edition. McGraw–Hill, New York, 1988. pp. 519-522.

13. ENGLER, O. and VALERIE, R. Introduction to Texture Analysis: Macrotexture, Microtexture, and Orientation Mapping. 2nd edn. CRC Press, Boton Raca, Florida, 2009. pp. 208–231.

14. BAI, D.Q., YUE, S., SUN, W.P., and JONAS, J.J. Effect of deformation parameters on the no-recrystallisation temperature in Nb-bearing steels. *Metallurgical Transactions A*, vol. 24A, 1993. pp. 2151–2159.

15. HAMADA, J., ONO, N., and INOUE, H. Effect of texture on r-value of ferritic stainless steel sheets. *ISIJ International*, vol. 51, no. 10, 2011. pp. 1740–1748. ◆